Soil Dynamics and Earthquake Engineering 164 (2023) 107639

Contents lists available at ScienceDirect

Soil Dynamics and Earthquake Engineering

journal homepage: www.elsevier.com/locate/soildyn

Multi-modal seismic control design for multi-storey buildings using cross-layer installed cable-bracing inerter systems: Part 1 theoretical treatment

Jianfei Kang [a], Songtao Xue [a,b], Liyu Xie [a,*], Hesheng Tang [a], Ruifu Zhang [a]

[a] Department of Disaster Mitigation for Structures, Tongji University, Shanghai, 200092, China
[b] Department of Architecture, Tohoku Institute of Technology, Sendai, 982-8577, Japan

ARTICLE INFO

Keywords:
Cross-layer
Cable-bracing inerter system
Multi-mode
Target mode control effect
Theoretical treatment

ABSTRACT

Many attempts have been made to improve the performance of buildings subjected to ground motions with a novel mechanic element, known as an inerter, thereby giving buildings more stability. Recently, a characteristic of the inerter system on controlling the target mode, called the target mode control effect, has been discovered. Considering the prospects of target mode control effect on controlling those buildings affected by multi-modal responses, in this study, cross-layer installed cable-bracing inerter systems (CICBISs) will be used for the multi-modal seismic control. For releasing the end torsion constraints demand of the ball-screw inerter and simplifying the CICBIS's realization, a self-balanced inerter is proposed. A multi-modal seismic control design strategy is proposed to determine the optimal parameters of CICBISs. The equivalent mass with a physical meaning of the multi-storey building with a CICBIS is proposed to quantify the control efficiency of the CICBIS's placement and determine the installation placement of CICBISs directly. A 20-story benchmark building is used to validate the design strategy. The results show that the CICBISs tuned to multi-modes through applying the proposed design strategy can simultaneously focus on controlling multiple target modes. Moreover, it is proved that under the same constraint on each device's control force, the designed CICBISs obtain a higher efficiency on suppressing seismic responses than those CICBISs for single-modal seismic control we proposed in the past and cross-three-layer installed tuned viscous mass dampers. Further sections of the study, including device tests on a self-balanced inerter's prototype and shake table tests on corresponding CIBCIS, will be offered in the following companion paper: Part 2 Experimental treatment.

1. Introduction

In the past two decades, numerical control strategies have been developed to suppress buildings vibrations [1–3]. Recently, researchers have increasingly emphasized the importance of a two-terminal inerter element [4–9]. The so-called inerter is a two-terminal mass element, of which the resistance force is proportional to the relative accelerations between its two terminals [4]. The inerter's prototype used in civil engineering originates from the liquid mass pump proposed by Kawamata [10] in 1973, when there was no clear definition of an inerter. The inerter's mass amplification effect means that the inerter's inertance (apparent mass) can be considerably larger than its physical mass obtained by using different amplification mechanisms [10–14]. As far as the author knows, the first and only inerter system used for seismic control in practice is the tuned viscous mass damper (TVMD) [15,16]. It contains a ball-screw inerter whose apparent mass is about 7124 times its physical mass. Meanwhile, when incorporated with other mechanical elements, such as springs and dampers, the inerter can further improve system's energy-dissipation efficiency. Such a benefit is called the damping enhancement effect. Indeed, the mass amplification effect and damping enhancement were not used intentionally until Ikago et al. [4] proposed the TVMD. Zhang et al. [9] discovered and proved the damping enhancement equation of inerter system and bridged the damping enhancement effect with the response mitigation ratio theoretically until recently. These inerter benefits facilitate the development of numerous vibration control technologies thereby improving their control efficiency and involving various types of structures, such as conventional buildings [17–20], multi-storey chimneys [21], wind

* Corresponding author.
E-mail address: liyuxie@tongji.edu.cn (L. Xie).

https://doi.org/10.1016/j.soildyn.2022.107639
Received 25 October 2022; Accepted 1 November 2022

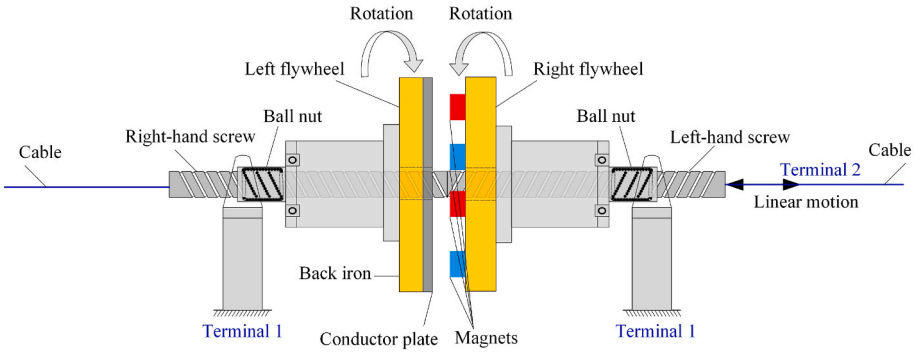

Fig. 1. Schematic of the self-balanced inerter.

towers [22,23], and storage tanks [24], etc.

Some scholars combined the inerter with traditional vibration control strategies such as tuned mass dampers (TMDs) [25–28], tuned liquid dampers [29,30], and isolators [31–34], to achieve better control performance or reduce the devices' weight with the help of inerter's mass amplification effect and damping enhancement effect.

Meanwhile, scholars have also demonstrated that using inerter systems alone provides higher efficiency over traditional damping devices [4,5,9,17]. By comparing the controlled systems' participation mode vectors and uncontrolled systems, Ikago et al. [35] proved the characteristic of the TVMD to increase the specified mode's damping ratio accurately without disturbing the mode's shape. Based on this characteristic, Ikago et al. [36] approximated the seismic response of the TVMD controlled structure through the primary structure with an increased specific modal damping ratio and proposed a simple design method for practical use. Considering the influence of non-resonant modes, Krenk et al. [37] proposed a calibration strategy for mass and inerter-based absorbers to suppress targeted modes. Wen et al. [38] distributed the inerter systems throughout the structure and tuned them to multiple modes, proving the high efficiency of the inerter system on multi-modal seismic control. Based on the master single-degree-of-freedom (SDOF) principle, Zhang et al. [39] proposed a method to control target modes using inerter systems and demonstrated that inerter systems can control target modes without affecting other modes.

The drawback in all these studies is that inerter systems are restricted to be installed between layers, which limits their utilization efficiency. Correspondingly, some researchers realized that using cables to connect the structure and damping systems can efficiently utilize cross-layer relative displacements, thus improving the damping systems' efficiency [40–42]. Benefitting from the cables' tension-only properties, cable-bracing damping systems break through the minimum cross-sectional limitation required to suppress buckling, making their deployment convenient. The cable-bracing damping systems can be installed directly on the facade of the building, or if necessary, the slabs can be drilled instead of removing the whole slabs. Coupling the cross-layer installed cable with the inerter system, a cross-layer installed cable-bracing inerter system (CICBIS) was proposed by authors, and its excellent economic efficiency was demonstrated through cost comparison [17,43]. It is worth noting that, in Refs. [17,43], only ideal inerter is considered in the CBIS to reveal their damping mechanism, while the drawback of cable being unable to provide the end torsion constraints required for the ball-screw inerter was ignored. Moreover, in Ref. [17], only controlling the first-order modal displacement response of the structure has been paid sufficient attention, where the proposed design approach tunes the CICBISs consistently to the vicinity of the first-order mode to obtain enough damping enhancement effect. It makes the designed CICBISs deficient in controlling buildings affected by multi-modes, which will be illustrated as a comparative case in the main text.

In this paper, a self-balanced inerter is put forward through remodeling the ball-screw inerter to overcome the drawback of cables ignored in Refs. [17,43] and simplify the CICBIS realization. Focusing on solving the deficiency of the CICBISs, proposed in the past research [17,43], in controlling multi-modal seismic responses of buildings, this study utilizes the target mode control mechanism to tune the CICBISs and show how CICBIS can achieve high economic efficiency considering multi-modal seismic control as well. This paper is organized as follows: first, a self-balanced inerter is introduced in detail. Then, the equivalent mass of a multi-storey building with a CICBIS is defined to quantify the relationship between the CICBIS's installation location and its efficiency in controlling the target mode. Subsequently, the multi-modal seismic control design strategy is proposed to control the multi-storey building's displacement and acceleration responses simultaneously. The design is based on the equivalent mass and the tuning concept. Finally, a 20-story benchmark building is used to validate the design strategy. Device tests carried out to verify the self-balanced inerter's zero end torque characteristic and shake table tests used to examine the response reduction effect of the CICBIS will be discussed in the accompanying paper.

2. Modeling and basic concepts of cable-bracing inerter system

2.1. Self-balanced inerter and cable-bracing inerter system

The ball-screw inerter is sufficient to get apparent mass required in civil engineering [15,16] with its mass amplification effect. However, because of the ball-screw inerter's displacement conversion mechanism (converting the linear motion into high-speed rotational motion through the ball nut and ball screw), additional torsion constraints are needed at its ends, which cannot be provided by the tension-only support, cable. To solve this problem, we developed the following inerter device, called a self-balanced inerter, which is able to release the end torsion constraints demand. The self-balanced inerter can be connected directly to the structure with the cables, which eliminates the need for auxiliary supports and simplifies the realization of the CBIS.

Fig. 1 depicts a schematic representation of the self-balanced inerter. A screw with different threads causes the flywheels of the inerter to rotate in opposite directions, enabling their torques to cancel each other out. By calculating the apparent mass of the inerter without end torque constraints, the importance of self-balancing when the end torque constraints are absent can be illustrated as follows. Assume that the torsional inertia of the left flywheel and its connect widgets is J_F; the right one is $\alpha_{SBI}J_F$; the torsional inertia of the screw is $\beta_{SBI}J_F$. The horizontal movement of the screw may be accompanied by rotation due to the inertial torque of the flywheels, as the cable is unable to provide end torque constraint. Set the angular acceleration of screw as $\ddot{\varphi}_s$ and the relative angular acceleration between the flywheel and screw as $\ddot{\varphi}$. According to the motion mechanism of the ball screw, $\ddot{\varphi}$ is determined by the relative displacement of the inerter's two terminals u_d and the lead length L_d:

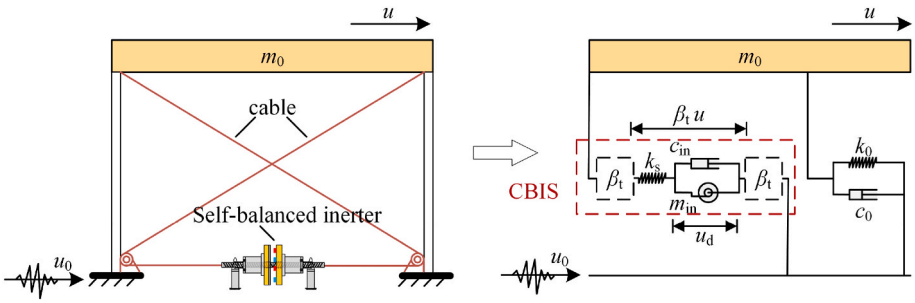

Fig. 2. Schematics of cable-bracing inerter system.

$$\ddot{\varphi} = \left(\frac{2\pi}{L_d}\right)\ddot{u}_d \tag{1}$$

Based on the torque balance, the following equation withstands:

$$\beta_{SBI} J_F \ddot{\varphi}_s = J_F\left(\ddot{\varphi} - \ddot{\varphi}_s\right) - \alpha_{SBI} J_F\left(\ddot{\varphi} + \ddot{\varphi}_s\right) \tag{2}$$

Thus, the angular acceleration of screw $\ddot{\varphi}_s$ is:

$$\ddot{\varphi}_s = \frac{1-\alpha_{SBI}}{(1+\alpha_{SBI}+\beta_{SBI})}\ddot{\varphi} \tag{3}$$

The axial forces are exerted by the flywheels are:

$$\begin{cases} P_L = \left(\frac{2\pi}{L_d}\right) J_F\left(\ddot{\varphi} - \ddot{\varphi}_s\right) = \frac{2\alpha_{SBI}+\beta_{SBI}}{1+\alpha_{SBI}+\beta_{SBI}}\left(\frac{4\pi^2 J_F}{{L_d}^2}\right)\ddot{u}_d \\ P_R = \left(\frac{2\pi}{L_d}\right)\alpha_{SBI} J_F\left(\ddot{\varphi} + \ddot{\varphi}_s\right) = \frac{2\alpha_{SBI}+\alpha_{SBI}\beta_{SBI}}{1+\alpha_{SBI}+\beta_{SBI}}\left(\frac{4\pi^2 J_F}{{L_d}^2}\right)\ddot{u}_d \end{cases} \tag{4}$$

Thus, the axial force exerted on the cable at the inerter's terminal 2, shown in Fig. 1, is:

$$P_F = P_L + P_R = \frac{4\alpha_{SBI}+\alpha_{SBI}\beta_{SBI}+\beta_{SBI}}{1+\alpha_{SBI}+\beta_{SBI}}\left(\frac{4\pi^2 J_F}{{L_d}^2}\right)\ddot{u}_d \tag{5}$$

It shows that the axial force of the self-balanced inerter is proportional to the relative acceleration at its two ends. The ratio is generally defined as apparent mass m_{in}:

$$m_{in} = \frac{4\alpha_{SBI}+\alpha_{SBI}\beta_{SBI}+\beta_{SBI}}{1+\alpha_{SBI}+\beta_{SBI}}\left(\frac{4\pi^2 J_F}{{L_d}^2}\right) \tag{6}$$

By submitting $\alpha_{SBI} = 0$ into Equation (3) and Equation (6), we get the angular acceleration of screw and the device's apparent mass, when the right flywheel disappears, which represents a conventional ball-screw inerter without end torsion constraints:

$$\ddot{\varphi}_s' = \frac{1}{(1+\beta_{SBI})}\ddot{\varphi} \tag{7}$$

$$m_{in}' = \frac{\beta_{SBI}}{1+\beta_{SBI}}\left(\frac{4\pi^2 J_F}{{L_d}^2}\right) \tag{8}$$

Notice that the torsional inertia of the screw is usually much smaller than the flywheel ($\beta_{SBI} \ll 1$). Resulting in the end torsion unconstrained ball screw inerter's apparent mass much smaller than the end torsion constrained one, whose apparent mass is known as $4\pi^2 J_F/{L_d}^2$ [4]. It means the screw rotate with the flywheel would make the apparent mass of the device decrease dramatically.

When the self-balance concept is taken into consideration and the right flywheel shown in Fig. 1 is added, we can submit $\alpha_{SBI} = 1$ into Equation (3) and Equation (6) and get the angular acceleration of screw equals to 0, the self-balanced inerter's apparent mass m_{SBI} is:

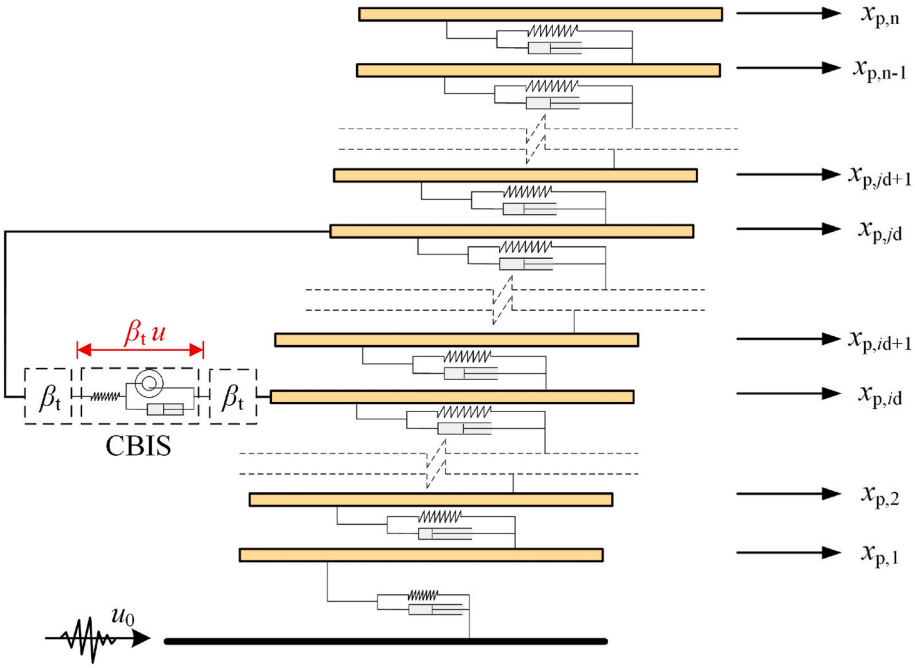

Fig. 3. Model of a multi-storey building with a CICBIS.

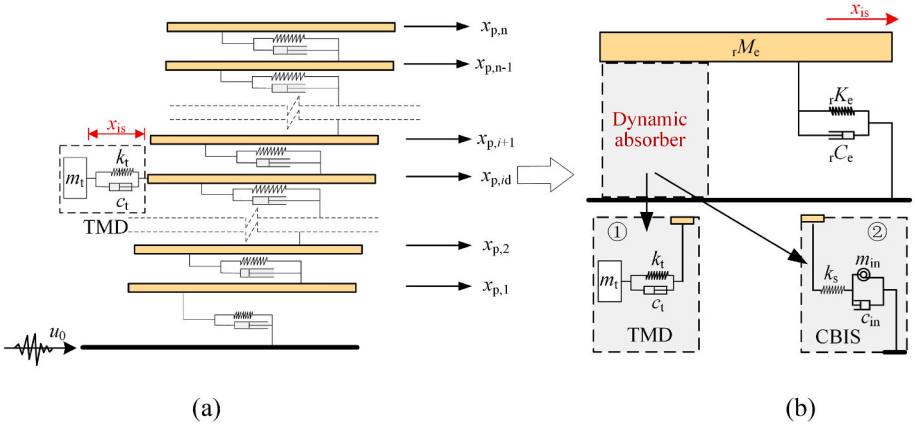

Fig. 4. Illustration of the equivalent mass definition: (a) multi-storey building.

$$m_{SBI} = 2 \cdot \left(\frac{4\pi^2 J_F}{L_d^{\,2}} \right) \tag{9}$$

To summarize: Compared with a traditional ball screw inerter, the self-balanced inerter not only has the self-balanced feature but can also obtain a doubled apparent mass owing to the simultaneous utilization of the inerter with flywheels.

Fig. 2 shows that the self-balanced inerter is directly connected to the structure with a pair of cables combined with some additional elements (such as the energy dissipation element and tuning stiffness). This is the simplest type of cable-bracing inerter system (CBIS). We discussed its efficiency on dynamic control in Ref. [17]. Notice that the energy dissipation element in parallel with the inerter can be achieved by installing back irons on one flywheel and permanent magnets on the other flywheel as shown in Fig. 1. Details are in Ref. [43]. The equivalent spring element is provided by adjusting the cables' stiffness. The governing equations of the SDOF structure controlled with CBIS in Fig. 2 subjected to the ground acceleration $\ddot{u}_0$ can be expressed as:

$$\begin{cases} m_0\ddot{u} + c_0\dot{u} + k_0 u + \beta_t F_{is} = -m_0\ddot{u}_0 \\ F_{is} = m_{in}\ddot{u}_d + c_{in}\dot{u}_d = k_s(\beta_t u - u_d) \\ \beta_t = \cos(\alpha_c) \end{cases} \tag{10}$$

where m_0, c_0 and k_0 are the mass, damping coefficient, and stiffness of the SDOF structure respectively; m_{in}, c_{in} and k_s are apparent mass, damping coefficient and tuning stiffness of the CBIS respectively; β_t is the displacement transition ratio, which represents the characteristic of the cable bracing system and its detailed definition can refer to Ref. [17]; α_c is the tilt angle of the cable.

2.2. Government equations of a multi-storey building with a CICBIS

Similar to Equation (10), the government equations of a multi-storey building with a CICBIS excited by ground acceleration $\ddot{u}_0$ can be expressed in the matrix form:

$$\mathbf{M}\ddot{\mathbf{X}} + \mathbf{C}\dot{\mathbf{X}} + \mathbf{K}\mathbf{X} = -\mathbf{M}\{\mathbf{E}\}\ddot{u}_0 \tag{11}$$

where $\mathbf{M}$, $\mathbf{C}$ and $\mathbf{K}$ are the mass, damping coefficient, and stiffness matrixes of the multi-storey building and the CBISs, respectively; $\mathbf{X}$ denotes the displacement vector of the controlled structure; $\mathbf{E}$ is the influential coefficient vector.

Taking a CBIS installed between the $i_d^{\,th}$ and $j_d^{\,th}$ layer of the multi-storey building as an example (see Fig. 3), the matrixes in Eq. (11) can be expressed as:

$$\mathbf{X} = \left\{ \mathbf{X}_p^T, x_{in} \right\}_{n+1,1}^{T}, \text{where } \mathrm{X_p} = \left\{ \mathrm{x_{p,1}}, \mathrm{x_{p,2}}, \cdots, \mathrm{x_{p,i}}, \cdots \mathrm{x_{p,n}} \right\} \tag{12}$$

$$\mathrm{M} = \begin{bmatrix} \mathrm{M_p} & 0 \\ 0 & \mathrm{m_d} \end{bmatrix}_{n+1,n+1}, \text{where } \mathrm{M_p} = \mathrm{diag}\left\{ \mathrm{m_{p,1}}, \mathrm{m_{p,2}}, \cdots, \mathrm{m_{p,i}}, \cdots \mathrm{m_{p,n}} \right\} \tag{13}$$

$$\mathrm{C} = \begin{bmatrix} \mathrm{C_p} & 0 \\ 0 & \mathrm{c_d} \end{bmatrix}_{n+1,n+1}, \text{where } \mathrm{C_p} = \mathrm{T^T diag}\left\{ \mathrm{c_{p,1}}, \mathrm{c_{p,2}}, \cdots, \mathrm{c_{p,i}}, \cdots \mathrm{c_{p,n}} \right\} \mathrm{T^T} \tag{14}$$

$$\mathrm{K} = \begin{bmatrix} \mathrm{K_p} + \mathrm{r_c k_s r_c}^{\mathrm{T}} & -\mathrm{r_c k_s} \\ -\mathrm{k_s r_c}^{\mathrm{T}} & \mathrm{k_s} \end{bmatrix}_{n+1,n+1}, \text{where } \mathbf{K_p} = \mathbf{T}^T \mathrm{diag}\left\{ k_{p,1}, k_{p,2}, \cdots, k_{p,i}, \cdots k_{p,n} \right\} \mathbf{T}^T \tag{15}$$

$$\{\mathbf{E}\} = \{1, 1, \cdots, 1, 0\}_{n+1}^{T}, \mathbf{T} = \begin{bmatrix} 1 & & & \\ -1 & 1 & & \\ & \ddots & \ddots & \\ & & -1 & 1 \end{bmatrix}_{n \times n} \tag{16}$$

Among the above equations, $x_{p,i}$ is the i^{th} layer's displacement of the primary structure relative to the ground; $m_{p,i}$, $c_{p,i}$, and $k_{p,i}$ are the i^{th} layer's mass, damping coefficient, and stiffness of the primary structure, respectively; $\mathbf{T}$ denotes the matrix used to convert the displacement relative to the ground into the displacement between layers; r_c is the vector representing the installation location of the CBIS:

$$r_c = \begin{cases} \{0, \cdots, -\beta_t, \cdots, \beta_t, \cdots, 0\}_{n\times 1}^{T} \quad i_d \quad j_d & i_d \neq 0 \\ \{0, \cdots, \beta_t, \cdots, 0\}_{n\times 1}^{T} \quad j_d & i_d = 0 \text{ (grounded)} \end{cases} \tag{17}$$

Extending x_{in}, m_d, c_d, k_s, and r_c in Eqs. 12–17 to corresponding matrixes can also describe the situation when multiple CBISs are installed, the detailed matrixes for multiple CBISs are shown in appendix A.

2.3. Equivalent mass with a physical meaning of the multi-storey building with a CICBIS

A previous study [39] has found that well-tuned inerter systems are well placed to avoid effects on modes other than their control target. Determining the optimal installation position of CICBISs targeting different modes one by one, which can simplify the optimization of multi-CICBISs significantly, therefore, becomes possible. Through analogy with the equivalent mass used by Seto [44] in the design

procedure for the TMD, we defined the equivalent mass with the physical meaning of the multi-storey building with a CICBIS to quantify the relationship between the CICBIS's placement and its control efficiency on the target mode. Based on the modal decomposition process [45,46], the modal responses of a controlled multi-storey building can be represented with an equivalent SDOF system controlled by corresponding CBIS targeted on the mode:

$$\begin{cases} \{{}_r\varphi\}^T\mathbf{M}_\mathrm{p}\{{}_r\varphi\}{}_r\alpha_p + \{{}_r\varphi\}^T\mathbf{C}_\mathrm{p}\{{}_r\varphi\}{}_r\alpha_p + \{{}_r\varphi\}^T\mathbf{K}_\mathrm{p}\{{}_r\varphi\}\alpha_p + \{{}_r\varphi\}^T r_\mathrm{c} k_\mathrm{d} r_\mathrm{c}^T\{{}_r\varphi\}\left({}_r\alpha_\mathrm{p} - {}_r\alpha_\mathrm{d}\right) = 0 \\ \{{}_r\varphi\}^T r_\mathrm{c} m_\mathrm{d} r_\mathrm{c}^T\{{}_r\varphi\}{}_r\ddot{\alpha}_\mathrm{d} + \{{}_r\varphi\}^T r_\mathrm{c} c_\mathrm{d} r_\mathrm{c}^T\{{}_r\varphi\}{}_r\dot{\alpha}_\mathrm{d} + \{{}_r\varphi\}^T r_\mathrm{c} k_\mathrm{d} r_\mathrm{c}^T\{{}_r\varphi\}\left({}_r\alpha_\mathrm{d} - {}_r\alpha_\mathrm{p}\right) = 0 \end{cases} \tag{18}$$

where, ${}_r\varphi$, ${}_r\alpha_\mathrm{p}$, and ${}_r\alpha_\mathrm{d}$ are rth modal shape vector, primary structure's modal displacement, and the inerter's modal displacement, respectively. The left subscript r denotes the rth mode.

However, the modal shape vector only reflects the proportional relationship between each layer's displacements, which can be scaled arbitrarily. It means the parameters of the equivalent SDOF structure obtained according to the modal shape vector, such as mass, damping coefficient, and stiffness, are uncertain. To make sure the relationship between the CICBIS's placement and its control efficiency on the target mode can be quantified, the scale factor of the modal shape vector ${}_r\varphi$ should be determined. Herein, based on the principle of making the equivalent SDOF modal displacement ${}_r\alpha_\mathrm{p}$ equal to the inerter system's displacement, x_is, as shown in Fig. 4, the modal shape vector, ${}_r\varphi$, is scaled as follows:

$${}_r\overline{\varphi} = \frac{1}{{}_r\varphi^T r_{\mathrm{c},r}}\{{}_r\varphi\} \tag{19}$$

where ${}_r\overline{\varphi}$ is the scaled modal shape vector; $r_{\mathrm{c},r}$ is the installation location vector of the CICBIS used to control the r^{th} mode.With a TMD and (b) controlled equivalent SDOF system.

According to the modal decomposition process, equivalent parameters of the multi-storey building with a CICBIS are related to the modal shape vector ${}_r\varphi$ and the installation location vector $r_{\mathrm{c},r}$ of the CICBIS:

$$\begin{aligned} {}_rM_e(r_{\mathrm{c},r}) &= \frac{1}{r_{\mathrm{c},r}^T\,{}_r\varphi}\{{}_r\varphi\}^T\mathbf{M}_\mathrm{p}\{{}_r\varphi\}\frac{1}{{}_r\varphi^T r_{\mathrm{c},r}} \\ {}_rC_e(r_{\mathrm{c},r}) &= \frac{1}{r_{\mathrm{c},r}^T\,{}_r\varphi}\{{}_r\varphi\}^T\mathbf{C}_\mathrm{p}\{{}_r\varphi\}\frac{1}{{}_r\varphi^T r_{\mathrm{c},r}} \\ {}_rK_e(r_{\mathrm{c},r}) &= \frac{1}{r_{\mathrm{c},r}^T\,{}_r\varphi}\{{}_r\varphi\}^T\mathbf{K}_\mathrm{p}\{{}_r\varphi\}\frac{1}{{}_r\varphi^T r_{\mathrm{c},r}} \end{aligned} \tag{20}$$

where ${}_rM_e$, ${}_rC_e$, and ${}_rK_e$ are the r^{th} modal equivalent mass, damping coefficient, and stiffness, respectively, which are functions of the installation location vector $r_{\mathrm{c},r}$.

Indeed, the equivalent SDOF determined according to scaled modal shape vector has the characteristic of keeping the parameters of the inerter system in CICBIS unchanged. Thus, those conclusions pertaining to controlling an SDOF structure using inerter systems can be directly used to determine the actual optimal parameter demands for controlling the target mode's responses in multi-storey buildings. Moreover, the change of installation location and target control mode only results in proportional scale of the equivalent SDOF structure. Obviously, the smaller the physical equivalent mass denoting the smaller structure, the lower the control device demand. In other words, if a inerter system were installed at the location leading to a smaller physical equivalent mass of the multi-storey buildings, its control effect on the target modal equivalent SDOF structure would be better.

3. Optimal strategy of multi-modal seismic control

3.1. Placement and parameter design of the CICBIS

For the CICBISs utilized to control the seismic vibration of a multi-storey building, it is essential to determine its targeted control modes, placement, and parameters. By performing the initial analysis of the

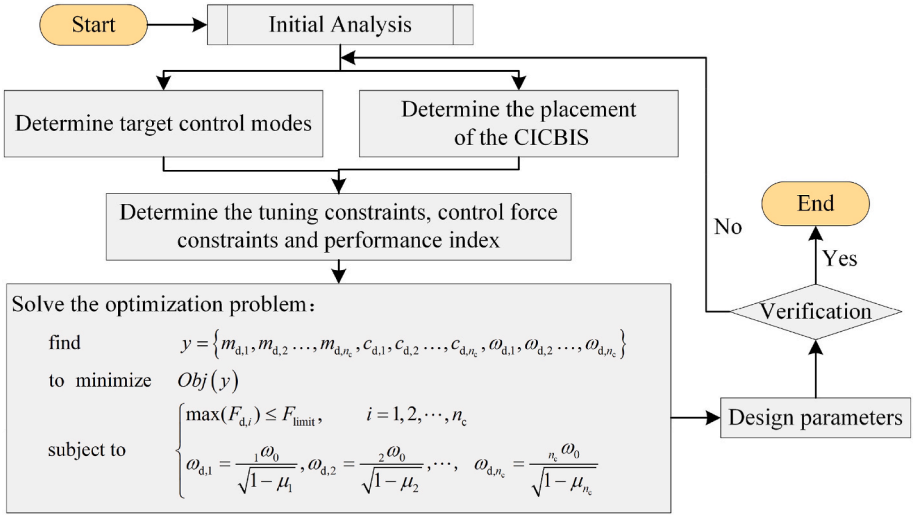

Fig. 5. Design flowchart of optimal multimode control of CICBISs.

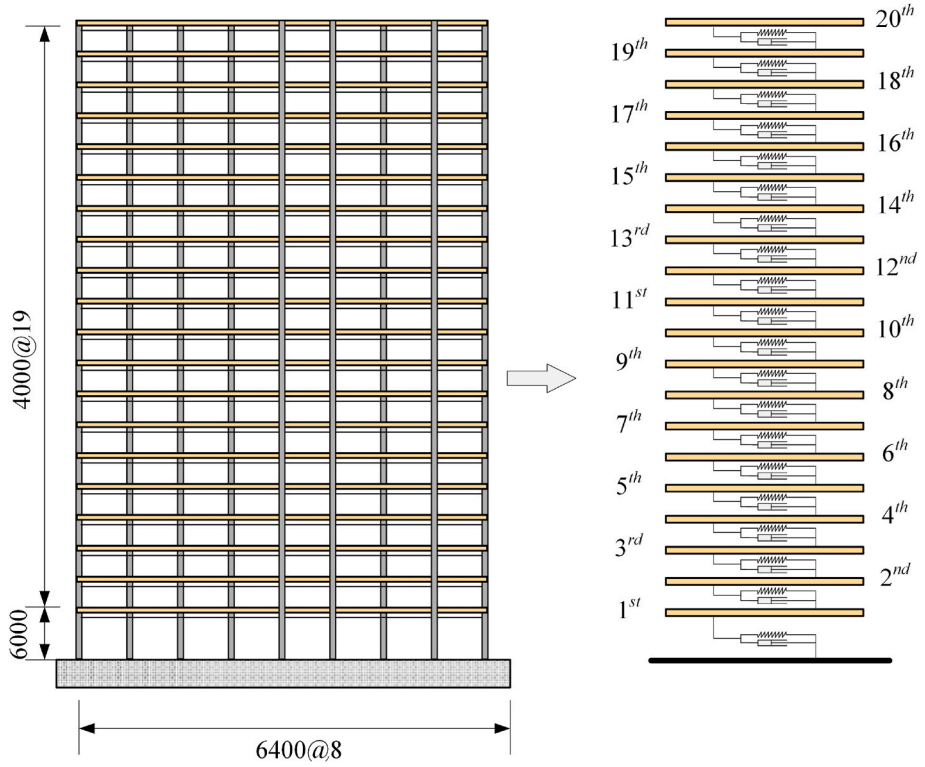

Fig. 6. Benchmark structure: A 20-story steel building provided by JSSI.

uncontrolled structure, the targeted control modes are initially determined based on the modal mass participation factor [21,47,48]. According to inerter system's target mode control effect, the well-tuned CICBIS would make less effect on the modes other than the target mode. Therefore, the placements of CICBISs for controlling different modes can determined one by one through minimizing the equivalent mass defined in Eq. (20), which will lead to the maximum CICBISs utilization efficiency. Assuming the less change on the modal shape vector would made by installing well-tuned inerter systems, the modal shape vector of the uncontrolled structure is directly used in Eq. (20) to avoid iterative calculations.

According to the configuration of the CICBIS, the design parameters must be determined through optimization, as follows:

$$y=\left\{m_{\mathrm{d},1},m_{\mathrm{d},2}\ldots,m_{\mathrm{d},n_{\mathrm{c}}},c_{\mathrm{d},1},c_{\mathrm{d},2}\ldots,c_{\mathrm{d},n_{\mathrm{c}}},\omega_{\mathrm{d},1},\omega_{\mathrm{d},2}\ldots,\omega_{\mathrm{d},n_{\mathrm{c}}}\right\} \tag{21}$$

where n_{c} is the number of targeted control modes; $m_{\mathrm{d},i}$, $c_{\mathrm{d},i}$, and $\omega_{\mathrm{d},i}$ denote the apparent mass, damping coefficient, and frequency of the CICBIS, respectively. Each control mode is used to control the i^{th} mode. The frequency, $\omega_{\mathrm{d},i}$, can be calculated as follows:

$$\omega_{\mathrm{d},i}=\sqrt{\frac{k_{\mathrm{s},i}}{m_{\mathrm{d},i}}} \tag{22}$$

where $k_{\mathrm{s},i}$ is the tuning stiffness of the CICBIS used to control the i^{th} mode.

For engineering practice, while controlling the seismic response, the price of the CICBIS must be constrained to a reasonable range. It is well known that a damping device's price is closely related to its control force [6–8]. Thus, the optimum design problem of the CICBISs formulated herein is subjected to the maximum response control force constraint; therefore, one must:

$$\begin{aligned}&\text{find}\quad y=\left\{m_{\mathrm{d},1},m_{\mathrm{d},2}\ldots,m_{\mathrm{d},n_{\mathrm{c}}},c_{\mathrm{d},1},c_{\mathrm{d},2}\ldots,c_{\mathrm{d},n_{\mathrm{c}}},\omega_{\mathrm{d},1},\omega_{\mathrm{d},2}\ldots,\omega_{\mathrm{d},n_{\mathrm{c}}}\right\}\\&\text{to minimize}\quad Obj(y)\\&\text{subject to}\quad\begin{cases}\max\left(F_{\mathrm{d},i}\right)\le F_{\mathrm{limit}},i=1,2,\cdots,n_{\mathrm{c}}\\\omega_{\mathrm{d},1}=\dfrac{{}_1\omega_0}{\sqrt{1-\mu_1}},\omega_{\mathrm{d},2}=\dfrac{{}_2\omega_0}{\sqrt{1-\mu_2}},\cdots,\omega_{\mathrm{d},n_{\mathrm{c}}}=\dfrac{{}_{n_{\mathrm{c}}}\omega_0}{\sqrt{1-\mu_{n_{\mathrm{c}}}}}\end{cases}\end{aligned} \tag{23}$$

where $Obj(y)$ denotes the design objective, representing the control performance of the CICBISs; $F_{\mathrm{d},i}$ and F_{limit} are the control force of the CICBIS used to control the i^{th} mode and the maximum response control force limitation, respectively; The constraint on the frequency is to ensure the damping enhancement and target mode control effect of the inerter systems, which is also shown in Refs. [4,35]; μ_i is the inerter-mass ratio of the i^{th} CICBIS:

$$\mu_i=\frac{m_{\mathrm{d},i}}{{}_iM_e(r_{\mathrm{c}})}=\frac{m_{\mathrm{d},i}}{\frac{1}{r_{\mathrm{c},i}^T\,{}_i\varphi}\left\{{}_i\varphi\right\}^T\mathbf{M}_{\mathrm{p}}\left\{{}_i\varphi\right\}\frac{1}{{}_i\varphi^T r_{\mathrm{c},i}}} \tag{24}$$

For controlling the displacement and acceleration responses simultaneously, the objective function $Obj(y)$ is chosen to be a combination of displacement and acceleration responses of the controlled structure:

$$Obj(y)=\alpha\frac{\theta_{\max}(y)}{\theta_{0,\max}}+(1-\alpha)\frac{a_{\max}(y)}{a_{0,\max}} \tag{25}$$

where, $\theta_{0,\max}$ and $\theta_{0,\max}$ are the uncontrolled and controlled root mean square (RMS) story drift ratio, respectively. Meanwhile, $a_{0,\max}$ and $a_{0,\max}$ are the uncontrolled and controlled RMS acceleration, respectively. Hence, $\alpha\in[0,1]$ is the weight, representing the significant of the displacement.

Table 1
Modal properties of the Benchmark structure.

Mode	Period (s)	Circular frequency (rad/s)	Mass participation coefficient
1	3.705	1.696	0.7661
2	1.412	4.450	0.1192
3	0.863	7.282	0.0470
4	0.622	10.098	0.0241
5	0.482	13.030	0.0129

3.2. Design flowchart

The proposed design procedure makes it possible to control multi-modal seismic response with high efficiency utilizing the CICBISs. The design flowchart in Fig. 5 can be summarized as follows:

Step 1: *Initial analysis of the uncontrolled multi-storey building.* Perform the modal analysis to obtain the frequency and the mass participation coefficient of the uncontrolled structure. Utilize the state-space approach [49] to calculate the RMS displacement and acceleration responses of the uncontrolled building excited with a zero-mean Gaussian white noise.

Step 2: *Determination of the targeted control modes and the placement of the CICBISs.* Choose the targeted control mode, ensuring the controlled modes' accumulative mass participation coefficient is at least 85%, referring to Refs. [21,47,48]. This determines the placement of the CICBIS used to control each mode according to the equivalent mass.

Step 3: *Determination of the performance objective and constraints.* The performance objective can be calculated according to Eq. (25). The RMS responses of the controlled structure are obtained through the state-space approach as well. The control force constraints are determined based on the performance requirement of the structure and simple iteration. The tuning constraints, referring to Refs. [17,35,39], are used to ensure the damping enhancement and target mode control effect.

Step 4: *Solving the optimization problem.* Solve the design parameters, y, for the optimization problem formulated by Eq. (23). The numerical optimization method is utilized herein to search through feasible parameters for its high efficiency.

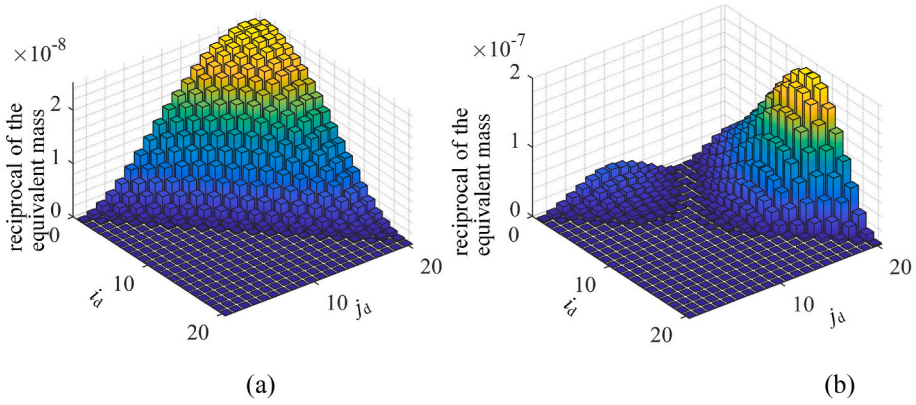

Fig. 7. Illustration of the equivalent masses (the effects of installation location).

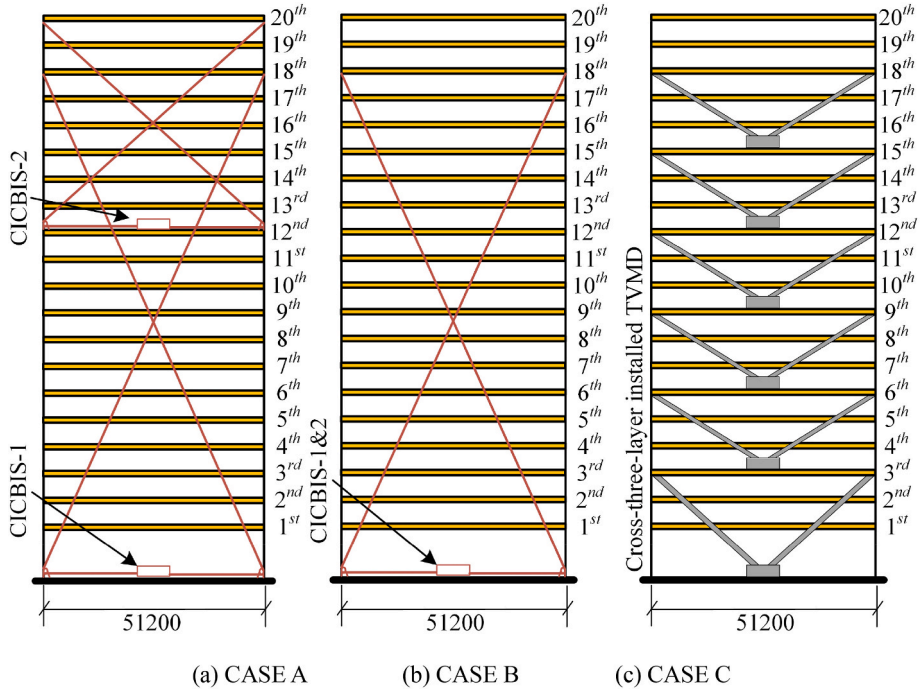

Fig. 8. Three design cases: (a) CICBISs for multi-modal seismic control, (b) CICBISs for single-modal seismic control, and (c) cross-three-layer installed TVMD.

Table 2
Optimal design parameters of each design case.

	Apparent mass ($\times 10^3$ kg)	Damping coefficient (kN/m/s)	Stiffness (kN/m)	Number of devices
CASE A	1375.826	1008.087	4098.802	1
	1267.809	5101.630	31795.162	1
CASE B	2174.902	2706.416	7023.575	2
CASE C	5297.621	5256.890	16366.824	6

Step 5: *Verifications of the CICBIS performance.* Calculate the frequency response functions (FRFs) to verify the multi-modal control effect of the designed CICBISs. Conduct the time history analysis to check the performance of the controlled structure. If the controlled structural responses exceed the limitation, go back to Step 2 and modify the targeted control mode, the performance objective, and the control force constraints.

4. Case studies

4.1. Modal information and initial analysis

To verify the design of the CICBISs for multi-modal seismic control of a multi-storey building, we utilized a 20-story Benchmark structure provided by the Japan Society for Seismic Isolation (JSSI) [50] as an example. The geometric information of this Benchmark building is shown in Fig. 6. A constant 2% modal damping is assumed for all modes when assembling the damping matrix $\mathbf{C}_p$. Through the initial analysis of the uncontrolled structure, the modal properties are listed in Table 1. The accumulative mass participation coefficient of the first two modes is almost 90%, i.e., more than 85%. Therefore, the first and the second modes were chosen as the targeted control mode.

The first and second modal equivalent masses of the Benchmark structure with a CICBIS were calculated according to Eq. (20). Fig. 7 shows the equivalent masses for all possible placements of the CICBIS. The x-axes and y-axes of the histograms shown in Fig. 7 denote the inerter system installation and cable anchor layers. In the histograms, the z-axis represents the reciprocal of the equivalent mass to observe more effectively. Therefore, for the first mode, the minimum equivalent mass was obtained through installing the CICBIS between the ground and the 18th layer. For the second mode, the CICBIS should install between the 12th and the 20th layer to obtain the minimum equivalent mass.

4.2. Parameter determination of the CICBISs

According to the initial analysis, we can conclude that installing the CICBISs, as shown in Fig. 8, can obtain its maximum utilization efficiency, which is defined as CASE A. Assuming the acceleration response is as important as the displacement, the weight α equals to 0.5 as example [51]. Thus, the optimization problem of CASE A can be expressed as follows:

$$\begin{aligned} &\text{find} \quad y = \left\{m_{\mathrm{d},1}, m_{\mathrm{d},2}, c_{\mathrm{d},1}, c_{\mathrm{d},2}, \omega_{\mathrm{d},1}, \omega_{\mathrm{d},2}\right\} \\ &\text{to minimize} \quad 0.5\frac{\theta_{\max}(y)}{\theta_{0,\max}} + 0.5\frac{a_{\max}(y)}{a_{0,\max}} \\ &\text{subject to} \quad \begin{cases} \max\left(F_{\mathrm{d},i}\right) \le F_{\mathrm{limit}}, i = 1,2 \\ \omega_{\mathrm{d},1} = \dfrac{1.696}{\sqrt{1-\mu_1}}, \omega_{\mathrm{d},2} = \dfrac{4.450}{\sqrt{1-\mu_2}} \end{cases} \end{aligned} \tag{26}$$

For illustrating the seismic response control efficiency of the designed multi-modal CICBISs (CASE A), Fig. 8 presents two more design cases compared with CASE A. CASE B is used to illustrate the advantages of designed multi-modal CICBISs compared to the single-modal CICBIS proposed in the Past [17], denoting the CICBISs for controlling the single-modal seismic control of the multi-storey building. In CASE B, two CICBISs are both installed between the ground and the 18th layer. CASE C represents the cross-three-layer installed TVMD, which has been discussed in Ref. [52]. CASE C is used to explain the high efficiency of CBIS compared to the traditional TVMD. Note that during the design procedure, the control force limitation for each inerter system of CASE A, CASE B, and CASE C are kept the same.

By solving the optimization problems, each design case's design parameters are listed in Table 2. Meanwhile, by submitting the optimal design parameters into Eq. (18), we obtained the performance indexes of CASE A, CASE B, and CASE C, which are 0.608, 0.669, 0.690, respectively. This means that the CICBISs designed according to multi-modal control are the best for reducing the responses under the same control force constraint. The maximum displacement responses of CASE A,

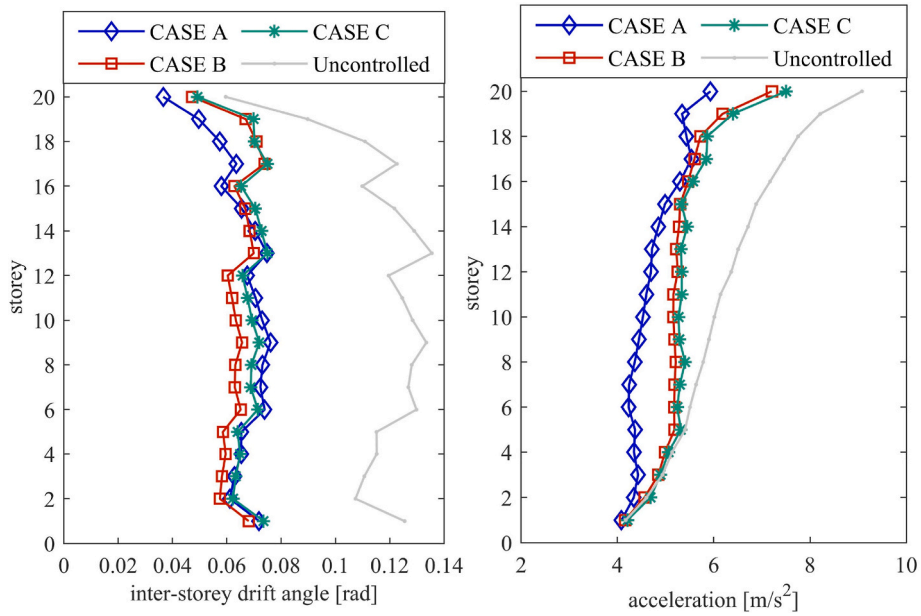

Fig. 9. RMS responses of the controlled and uncontrolled structures.

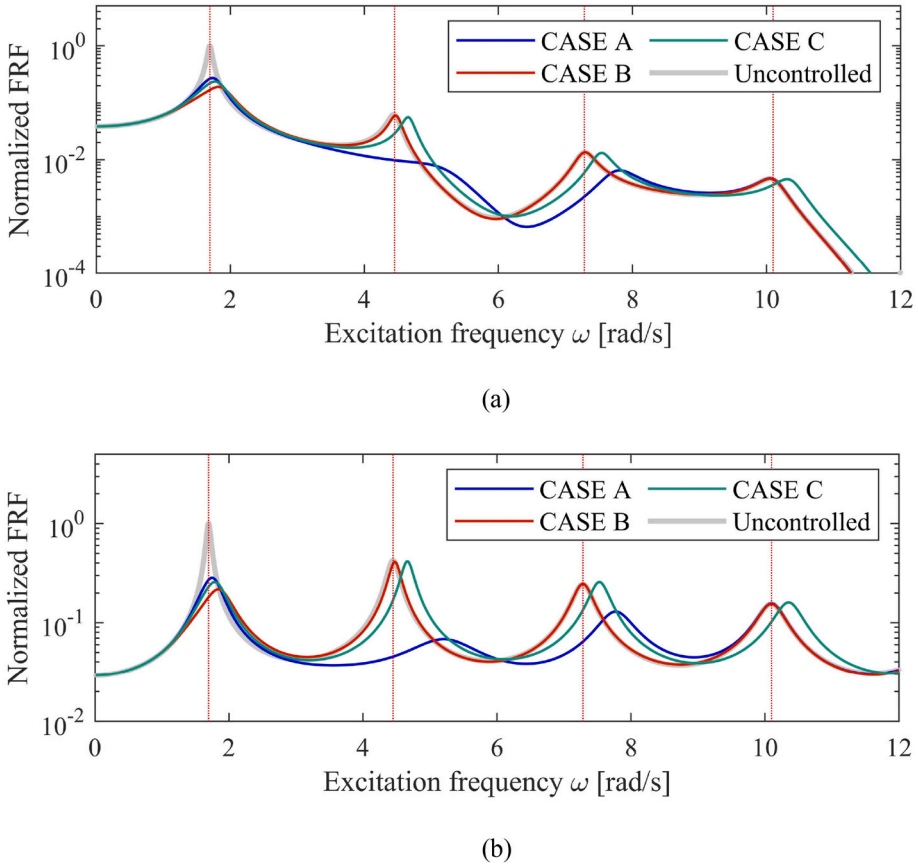

Fig. 10. Normalized FRFs for uncontrolled and controlled benchmark building. (a) Displacement of the top floor and (b) absolute acceleration of the top floor.

Table 3
Comparative periods and damping ratios of uncontrolled and controlled structure.

Mode	Uncontrolled		CASE A		CASE B	
	Period (s)	Damping ratio	Period (s)	Damping ratio	Period (s)	Damping ratio
1	3.705	0.020	3.814	0.160	4.005	0.279
			3.611	0.089	3.390	0.110
2	1.412	0.020	1.658	0.367	1.407	0.020
			1.239	0.100		
3	0.863	0.020	0.824	0.034	0.863	0.020
4	0.622	0.020	0.622	0.020	0.622	0.020
5	0.482	0.020	0.482	0.020	0.482	0.020

Mode	CASE C	
	Period (s)	Damping ratio
1	3.925	0.216
	3.997	0.297
	3.929	0.294
	3.883	0.292
	3.861	0.290
	3.840	0.289
	3.481	0.098
2	1.348	0.020
3	0.835	0.020

CASE B, and CASE C are 56.16%, 54.53%, and 55.31% of the uncontrolled structure, respectively. This reflects the similarity in their displacement control effect. Fig. 9 shows the significant advantage of CASE A in acceleration response control. The acceleration responses of CASE B and CASE C are 1.21 and 1.26 times the response of CASE A. In other words, if CASE B and CASE C are designed to have a similar control effect to that of CASE A, the control force limitation needs to be relaxed, which requires a price increment.

Notably, the parameters requirement of CASE A, shown in Table 2, is the least among these three design cases. The total apparent mass used in CASE A is around 3000 tons, which is only 60.78% and 8.32% of that used in CASE B and CASE C, respectively. This reflects the high efficiency of the CICBISs compared with traditional TVMD.

4.3. Verification of the efficiency of CICBISs

In this section, frequency response functions (FRFs) are calculated first to verify the multi-modal control effect and second to explain its significance as it relates to this paper's previous multi-modal control analysis in Section 3. The displacement and acceleration FRFs of the controlled and uncontrolled structures are shown in Fig. 10 where all the controlled structure's FRFs are normalized by the uncontrolled ones, and the red dashes denote the frequencies of the primary system in order. The FRFs of CASE A, CASE B, CASE C, and uncontrolled structure are illustrated using blue, red, green, and gray lines, respectively.

The FRFs of the uncontrolled structure show that the displacement response is mainly affected by the first mode, while the acceleration response is affected by multi-modes. Fig. 10 shows that CASE B and CASE C are slightly better than CASE A on controlling the first modal response. Moreover, CASE A controls the first three modes while CASE B and CASE C cannot control the second and higher mode responses. Although the trends shown by the displacement and acceleration FRFs are the same, the displacement and acceleration are affected differently by each mode. Higher-order mode effects on the acceleration response leads to significant differences in the RMS acceleration responses of CASE A, CASE B, and CASE C. It can be concluded that tuning CASE B and CASE C to the first mode of the structure gives them the ability to

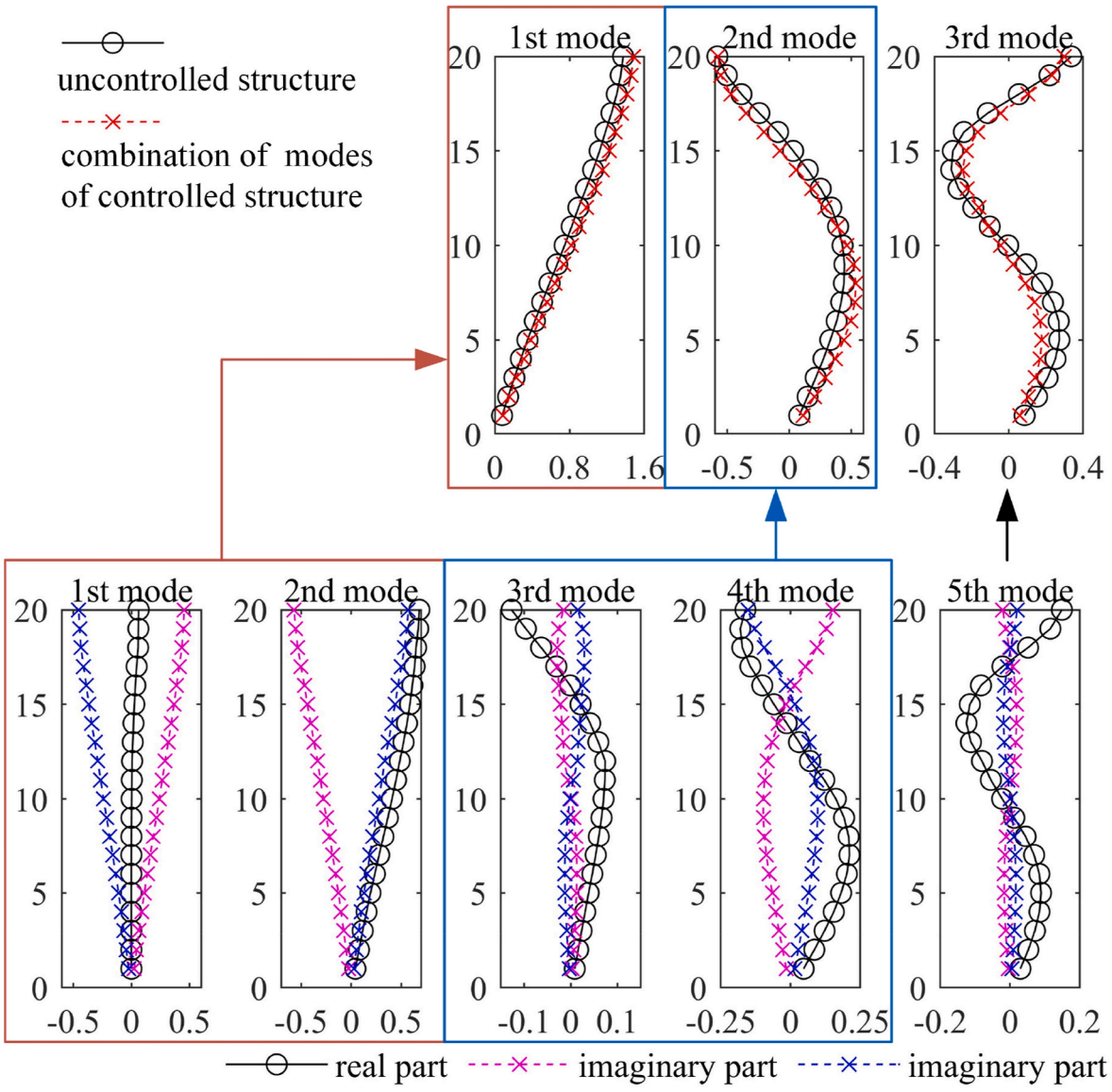

Fig. 11. Comparison of the participation mode vectors of the uncontrolled structure and CASE A (red lines) aligning with first uncontrolled structure's participation mode vector (black lines).

focus on controlling the first modal response, leading to a better displacement control effect. Utilizing its control effects on the first three modal responses, CASE A can be used to control the acceleration responses without severely deteriorating its displacement control effect.

Furthermore, the complex modal analysis of the controlled structure is performed to verify the high efficiency of CASE A. The periods and obtained damping ratios are listed in Table 3. The controlled structure has additional modes in the vicinity of the target modes because the inerter systems are tuned to the target modes. This additional activity is also known as an uncontrolled structure's modal splitting [35]. In CASE A, CASE B, and CASE C, the first-order mode of the uncontrolled structure split into 2, 2, and 7 modes, respectively. On average, the first-order modal damping ratios of CASE A, CASE B, and CASE C are 6.225, 9.725, and 12.686 times that of the uncontrolled structure, respectively. This is consistent with the advantages of CASE B and CASE C on controlling the first-order modal responses compared to CASE A shown in Fig. 10. Unlike CASE B and CASE C, the second and third-order modal damping ratios improved in CASE A as well. CASE A's second and third-order damping ratios are 11.675 times and 1.70 times, respectively, which is what they would be if uncontrolled. The influence of CICBIS in CASE A on the modal damping ratios, not counting the first to third modes, is almost negligible.

Meanwhile, Fig. 11 shows the participation mode vectors of the uncontrolled structure and CASE A obtained from modal analysis. When comparing the participation mode vectors, the invariance of the modal information can be observed. For example, the combination of the first and second participation mode vectors of CASE A (red dash line) is similar with the first uncontrolled structure's participation mode vector (solid black line). The similarity can be observed from other modes as well. Indeed, it is the splitting of modes without shape change significantly that ensures the reasonableness of the optimal placement of CICBIS obtained from uncontrolled structure modes.

The histogram in Fig. 12 compares the displacement and acceleration results of three different cases obtained from the time history analysis for each accelerogram. Herein, eight typical accelerograms are considered, containing an artificial accelerogram BCJ-L2 provided by the Building Center of Japan, and seven famous recorded earthquake accelerograms with different characteristics: 1) the Northbridge accelerogram, 2) the El Centro accelerogram, 3) the Kobe accelerogram, 4) the Chi-chi accelerogram, 5) the Loma Prieta accelerogram, 6) the

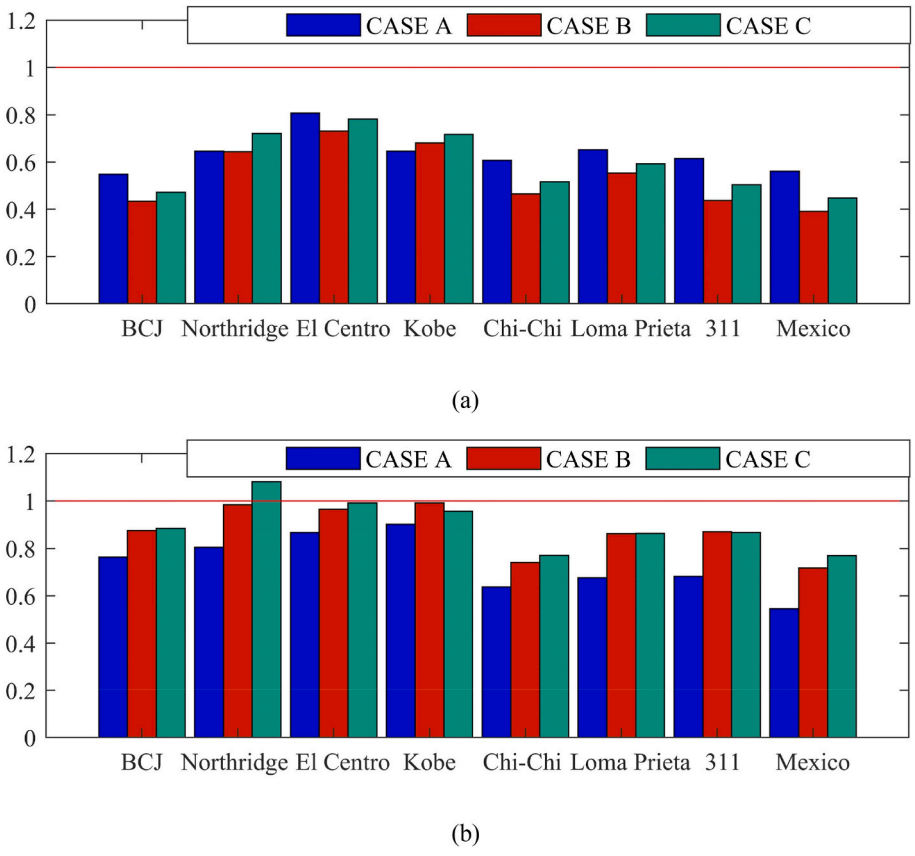

Fig. 12. Comparations of the benchmark structure under different accelerograms shown as (a) displacement and (b) acceleration.

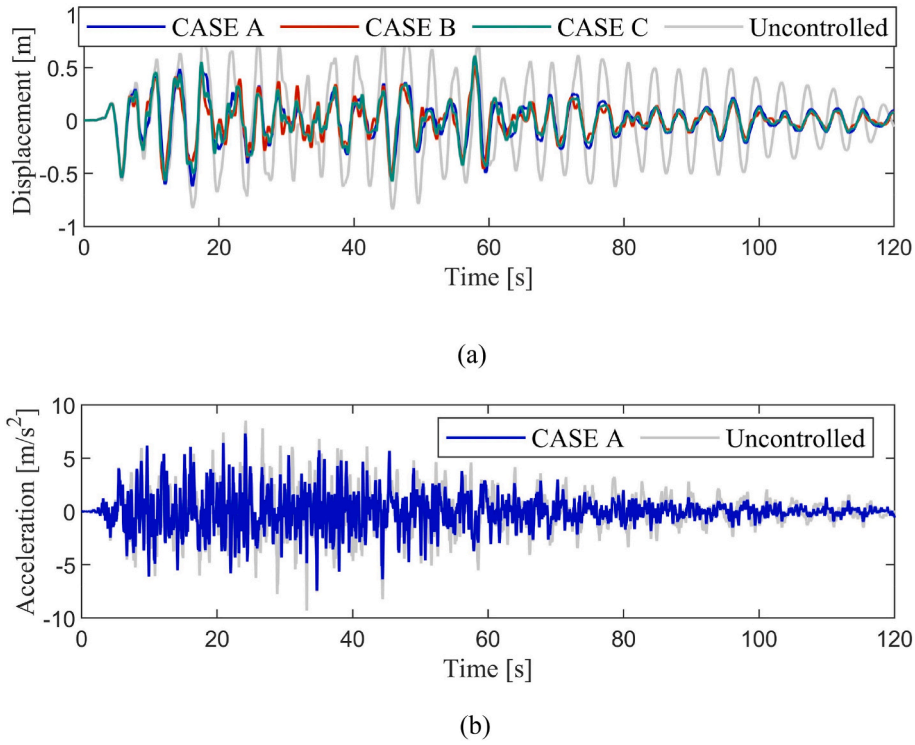

Fig. 13. Example responses of time history analysis (BCJ-L2). (a) Roof displacement of each case and (b) roof acceleration of CASE A and an uncontrolled structure.

Table 4
The damping enhancement factors.

Accelerograms	CASE A		CASE B	CASE C
	1st	2nd		
BCJ-L2	2.064	1.081	1.293	1.330
Northbridge	1.860	1.136	1.115	0.827
El Centro	1.939	1.107	1.285	1.334
Kobe	1.631	1.110	0.951	0.653
Chi-chi	2.081	1.091	1.340	1.497
Loma Prieta	1.995	1.099	1.282	1.386
Tohoku (311)	2.172	1.083	1.358	1.346
Mexico	2.137	1.078	1.375	1.440

Tohoku accelerogram (311), and 7) the Mexico accelerogram. Except for the Tohoku accelerogram recorded by the Tohoku University, other famous accelerograms are from the Pacific Earthquake Engineering Research Center database. The comparisons in Fig. 12 are normalized by the uncontrolled structural responses. All displacement results of three different cases are smaller than the one reflecting the displacements that were suppressed successfully. On average, the normalized displacement results of CASE A, CASE B, and CASE C are 0.635, 0.542, and 0.594, respectively, which is consistent with the previous discussion on the displacement control effect.

Note that the acceleration results of three cases in Fig. 12 show the failure of acceleration control using CASE B and CASE C. CASE C's acceleration is even larger than the uncontrolled one for the Northbridge accelerogram, which may be attributed to the earthquake's high-frequency components. Meanwhile, CASE A still shows an excellent control effect on the acceleration. On average, the normalized acceleration result of CASE A is 0.734. An example time history analysis of these three design cases is shown in Fig. 13.

In addition to the control effect of the inerter systems, the damping enhancement effect is another critical index to quantify the inerter systems' efficiency. As mentioned in Ref. [9], the damping enhancement factor Γ can be defined as:

$$\Gamma = \frac{\text{RMS displacement of the damping element}}{\text{RMS displacement of the inerter system}} \tag{27}$$

The damping enhancement factors of each case for different accelerograms are listed in Table 4. The deformation of the inerter systems and the damping elements of these three design cases for BCJ-L2 are shown as an example in Fig. 14. Notably, the damping enhancement factors of the CICBISs used in CASE A are always larger than one, reflecting a robust damping enhancement effect. In CASE B and CASE C, the damping enhancement factors of CICBISs are relatively small, even for the Northbridge accelerogram and the Kobe accelerogram, the damping enhancement factors may be smaller than one. This is consistent with their failure to control the acceleration shown in Fig. 12. The lower damping enhancement factors of the CICBISs used to control the second mode of CASE A also explain the relatively higher damping coefficient requirement for the CIBCISs shown in Table 2.

5. Conclusions

This paper presents a study of the application of CICBISs in the multi-modal seismic control of multi-storey buildings and proposes a corresponding design strategy. The main conclusions are as follows:

(1) A self-balanced inerter is proposed to release the demand of the ball-screw inerter for end rotation constraints, enabling the inerter system to be supported by cables directly. This further simplifies the realization of CICBISs.
(2) By analogy to the TMD scheme, the definition of the equivalent mass with a physical meaning of the multi-storey building with a CICBIS is proposed to quantify the relationship between the inerter system's placement and its control efficiency on the target mode. Based on the equivalent SDOF, the optimal installation setup of CICBISs, whose equivalent mass is minimum and specified modal control efficiency, is highest is conceptually discussed. Furthermore, the installation location of the CICBIS for multi-modal control is directly determined from the initial analysis of the uncontrolled structure, which simplifies the design process and provides references for the design of multi-modal seismic response control devices.
(3) According to the results of the 20-story Benchmark structure, we verified that the proposed design strategy can generally achieve

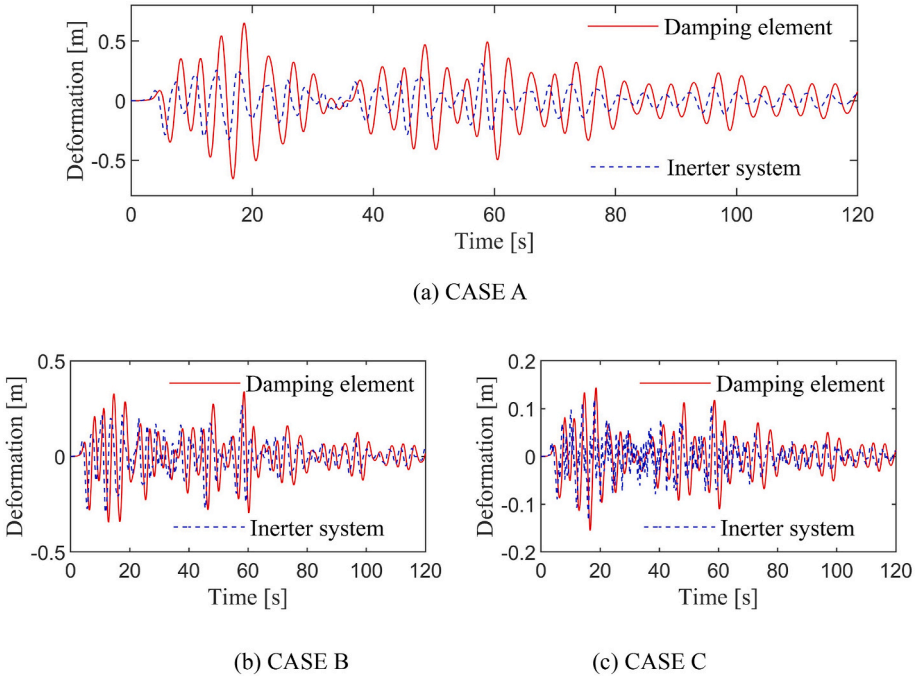

Fig. 14. The damping enhancement illustration (BCJ-L2).

target performance. The multi-mode control method obtains better performance in controlling the acceleration responses. Compared with traditional TVMD, the CICBIS is more efficient, which is reflected in the smaller parameter requirements under the same device's control force constraints. The CICBISs provide a novel way to realize multi-storey structure's seismic control at a lower cost.

Although the proposed method simplifies the analysis, it does have some shortcomings. The bending deformation of multi-storey buildings, which can affect CICBIS performance, is ignored. Only displacement and acceleration responses obtained from the elastic analysis are discussed here to represent the control performance of devices. More detailed finite element models are needed to investigate the CICBISs' control effect. We will address all these concerns in future research.

Funding

This study was supported by the National Key R&D Program of China (Grant No.2021YFE0112200), the Natural Science Foundation of Shanghai (Grant No. 20ZR1461800).

Declaration of competing interest

The authors declare that they have no known competing financial interests or personal relationships that could have appeared to influence the work reported in this paper.

Data availability

Data will be made available on request.

Appendix A

When considering n_d CBISs are used to control the multi-storey, the matrixes in Eq. (11) can be extended as follows:

$$\mathbf{X}=\left\{\mathbf{X}_p^T,\mathbf{X}_{in}\right\}^T_{n+n_d,1},\ \text{where}\ \mathbf{X}_{in}=\left\{x_{in,1},x_{in,2},\cdots,x_{in,i},\cdots x_{in,n_d}\right\} \tag{28}$$

$$\mathbf{M}=\begin{bmatrix}\mathbf{M}_p & 0\\ 0 & \mathbf{M}_d\end{bmatrix}_{n+n_d,n+n_d},\ \text{where}\ \mathbf{M}_d=\text{diag}\left\{m_{d,1},m_{d,2},\cdots,m_{d,i},\cdots m_{d,n_d}\right\} \tag{29}$$

$$\mathbf{C}=\begin{bmatrix}\mathbf{C}_p & 0\\ 0 & \mathbf{C}_d\end{bmatrix}_{n+n_d,n+n_d},\ \text{where}\ \mathbf{C}_d=\text{diag}\left\{c_{d,1},c_{d,2},\cdots,c_{d,i},\cdots c_{d,n_d}\right\} \tag{30}$$

$$\mathbf{K}=\begin{bmatrix}\mathbf{K}_p+\mathbf{R}_c\mathbf{K}_s{\mathbf{R}_c}^T & -\mathbf{R}_c\mathbf{K}_s\\ -\mathbf{K}_s{\mathbf{R}_c}^T & \mathbf{K}_s\end{bmatrix}_{n+n_d,n+n_d},\ \text{where}\ \mathbf{K}_s=\text{diag}\left\{k_{s,1},k_{s,2},\cdots,k_{s,i},\cdots k_{s,n_d}\right\} \tag{31}$$

$\mathbf{R}_c$ is the matrix representing the installation location of the CBISs, whose row elements represents the location of each CBIS.

References

[1] Housner GW, Bergman LA, Caughey TK, Chassiakos AG, Claus RO, Masri SF, et al. Structural control: past, present, and future. J Eng Mech 1997;123:897–971.
[2] Soong TT, Spencer BF. Supplemental energy dissipation: state-of-the-art and state-of-the-practice. Eng Struct 2002;24:243–59.
[3] Soong TT, Constantinou MC. Passive and active structural vibration control in civil engineering. Wien: Springer-Verlag; 2014.
[4] Ikago K, Saito K, Inoue N. Seismic control of single-degree-of-freedom structure using tuned viscous mass damper. Earthq Eng Struct D 2012;41:453–74.
[5] Lazar IF, Neild SA, Wagg DJ. Using an inerter-based device for structural vibration suppression. Earthq Eng Struct D 2014;43:1129–47.
[6] Pan C, Zhang R. Design of structure with inerter system based on stochastic response mitigation ratio. Struct Control Hlth 2018;25:e2169.
[7] Pan C, Zhang R, Luo H, Li C, Shen H. Demand-based optimal design of oscillator with parallel-layout viscous inerter damper. Struct Control Hlth 2018;25:e2051.
[8] Taflanidis AA, Giaralis A, Patsialis D. Multi-objective optimal design of inerter-based vibration absorbers for earthquake protection of multi-storey building structures. J Franklin I 2019;356:7754–84.
[9] Zhang R, Zhao Z, Pan C, Ikago K, Xue S. Damping enhancement principle of inerter system. Struct Control Hlth 2020:e2523.
[10] Kawamata S. Development of a vibration control system of structures by means of mass pumps. Tokyo, Japan: Institute of Industrial Science ,University of Tokyo; 1973.
[11] Swift SJ, Smith MC, Glover AR, Papageorgiou C, Gartner B, Houghton NE. Design and modelling of a fluid inerter. Int J Control 2013;86:2035–51.
[12] Makris N, Kampas G. Seismic protection of structures with supplemental rotational inertia. J Eng Mech 2016;142:04016089.
[13] Brzeski P, Lazarek M, Perlikowski P. Experimental study of the novel tuned mass damper with inerter which enables changes of inertance. J Sound Vib 2017;404:47–57.
[14] Sugiura K, Watanabe Y, Asai T, Araki Y, Ikago K. Experimental characterization and performance improvement evaluation of an electromagnetic transducer utilizing a tuned inerter. J Vib Control 2019;26:56–72.
[15] Sugimura Y, Goto W, Tanizawa H, Saito K, Nimomiya T. Response control effect of steel building structure using tuned viscous mass damper. In: The 15th world conference on earthquake engineering. Lisbon: Portugal; 2012.
[16] Watanabe Y, Ikago K, Inoue N, Kida H, Nakaminami S, Tanaka H, et al. Full-scale dynamic tests and analytical verification of a force-restricted tuned viscous mass damper. In: The 15th world conference on earthquake engineering. Lisbon: Portugal; 2012.
[17] Xue S, Kang J, Xie L, Zhang R, Ban X. Cross-layer installed cable-bracing inerter system for MDOF structure seismic response control. Appl Sci-Basel 2020;10:5914.
[18] De Domenico D, Ricciardi G, Zhang R. Optimal design and seismic performance of tuned fluid inerter applied to structures with friction pendulum isolators. Soil Dynam Earthq Eng 2020;132:106099.
[19] De Domenico D, Impollonia N, Ricciardi G. Soil-dependent optimum design of a new passive vibration control system combining seismic base isolation with tuned inerter damper. Soil Dynam Earthq Eng 2018;105:37–53.
[20] Garrido H, Curadelli O, Ambrosini D. Improvement of tuned mass damper by using rotational inertia through tuned viscous mass damper. Eng Struct 2013;56:2149–53.
[21] Zhang L, Xue S, Zhang R, Xie L. Simplified multimode control of seismic response of high-rise chimneys using distributed tuned mass inerter systems (TMIS). Eng Struct 2020;228:111550.
[22] Sarkar S, Fitzgerald B. Vibration control of spar-type floating offshore wind turbine towers using a tuned mass-damper-inerter. Struct Control Hlth 2020;27:e2471.
[23] Zhang R, Zhao Z, Dai K. Seismic response mitigation of a wind turbine tower using a tuned parallel inerter mass system. Eng Struct 2019;180:29–39.
[24] Jiang Y, Zhao Z, Zhang R, De Domenico D, Pan C. Optimal design based on analytical solution for storage tank with inerter isolation system. Soil Dynam Earthq Eng 2020;129:105924.
[25] Lara-Valencia LA, Farbiarz-Farbiarz Y, Valencia-González Y. Design of a tuned mass damper inerter (TMDI) based on an exhaustive search optimization for structural control of buildings under seismic excitations. Shock Vib 2020;2020:8875268.
[26] Díaz DAC. A comparative analysis on the seismic behavior of buildings using inerter-based devices: tuned Mass Damper Inerter (TMDI) and Tuned Inerter Damper (TID). Medellín, Colombia: Universidad Nacional de Colombia; 2020.

[27] Marian L, Giaralis A. Optimal design of a novel tuned mass-damper-inerter (TMDI) passive vibration control configuration for stochastically support-excited structural systems. Probabilist Eng Mech 2014;38:156–64.
[28] Caicedo D, Lara-Valencia L, Blandon J, Graciano C. Seismic response of high-rise buildings through metaheuristic-based optimization using tuned mass dampers and tuned mass dampers inerter. J Build Eng 2021;34:101927.
[29] Wang Q, Qiao H, De Domenico D, Zhu Z, Tang Y. Seismic response control of adjacent high-rise buildings linked by the Tuned Liquid Column Damper-Inerter (TLCDI). Eng Struct 2020;223:111169.
[30] Wang Q, Qiao H, De Domenico D, Zhu Z, Tang Y. Seismic performance of optimal Multi-Tuned Liquid Column Damper-Inerter (MTLCDI) applied to adjacent high-rise buildings. Soil Dynam Earthq Eng 2021;143:106653.
[31] Masnata C, Di Matteo A, Adam C, Pirrotta A. Assessment of the tuned mass damper inerter for seismic response control of base-isolated structures. Struct Control Hlth 2021;28:e2665.
[32] De Angelis M, Giaralis A, Petrini F, Pietrosanti D. Optimal tuning and assessment of inertial dampers with grounded inerter for vibration control of seismically excited base-isolated systems. Eng Struct 2019;196:109250.
[33] De Domenico D, Ricciardi G. Improving the dynamic performance of base-isolated structures via tuned mass damper and inerter devices: a comparative study. Struct Control Hlth 2018;25:e2234.
[34] Nakaminami S, Ikago K, Inoue N, Kida H. Response characteristics of a base-isolated structure incorporated with a force-restricted viscous mass damper damper. The 15th world conference on earthquake engineering. Lisbon: Portugal; 2012.
[35] Ikago K, Sugimura Y, Saito K, Inoue N. Modal response characteristics of a multiple-degree-of-freedom structure incorporated with tuned viscous mass dampers. J Asian Archit Build 2012;11:375–82.
[36] Ikago K, Sugimura Y, Saito K, Inoue N. Simple design method for a tuned viscous mass damper seismic control system. In: The 15th world conference on earthquake engineering. Lisbon: Portugal; 2012.
[37] Krenk S, Høgsberg J. Tuned resonant mass or inerter-based absorbers: unified calibration with quasi-dynamic flexibility and inertia correction. Proc Math Phys Eng Sci 2016;472:20150718.
[38] Wen Y, Chen Z, Hua X. Design and evaluation of tuned inerter-based dampers for the seismic control of MDOF structures. J Struct Eng 2017;143:04016207.
[39] Zhang R, Zhang L, Pan C, De Domenico D, Chen Q. Targeted modal response control of structures using inerter-based systems based on master oscillator principle. Int J Mech Sci 2021:106636.
[40] Sorace S, Terenzi G. The damped cable system for seismic protection of frame structures-Part II: design and application. Earthq Eng Struct D 2012;41:929–47.
[41] Sorace S, Terenzi G. The damped cable system for seismic protection of frame structures-Part I: general concepts, testing and modeling. Earthq Eng Struct D 2012;41:915–28.
[42] Aly AM, Zasso A, Resta F. On the dynamics of a very slender building under winds: response reduction using MR dampers with lever mechanism. Struct Des Tall Spec 2011;20:539–51.
[43] Xie L, Ban X, Xue S, Ikago K, Kang J, Tang H. Theoretical study on a cable-bracing inerter system for seismic mitigation. Appl Sci-Basel 2019;9:4096.
[44] Seto K. Dynamic vibration absorber and its applications. Tokyo,Japan: Corona Publishing Co., Ltd; 2010.
[45] Chopra AK. Dynamics of structures, A primer. Sunny buffalo. Earthquake Engineering Research Institute, State University of New York; 1981.
[46] Rana R, Soong TT. Parametric study and simplified design of tuned mass dampers. Eng Struct 1998;20:193–204.
[47] Chopra AK. Dynamics of structures : theory and applications to earthquake engineering. Englewood Cliffs (N.J): Prentice Hall; 1995.
[48] Palermo M, Silvestri S, Gasparini G, Trombetti T. Seismic modal contribution factors. B Earthq Eng 2015;13:2867–91.
[49] Lutes LD, Sarkani S. Random vibrations: analysis of structural and mechanical systems. Butterworth-Heinemann; 2004.
[50] Manual J. Manual for design and fabrication for passive vibration control of structures. 2005.
[51] Ji X, Zhang J, Ikago K, Chakraborty S, Kanno H. Tuned viscous mass damper (TVMD) coupled wall system for enhancing seismic performance of high-rise buildings. Eng Struct 2021;240:112307.
[52] Ogino M, Sumiyama T. Structural design of a high-rise building using tuned viscous mass dampers installed across three consecutive sotreys. In: The 12th international conference on computational structures technology. Scotland: Stirlingshire; 2014.